

Robotica

<http://journals.cambridge.org/ROB>

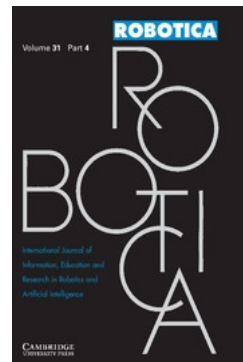
Additional services for **Robotica**:

Email alerts: [Click here](#)

Subscriptions: [Click here](#)

Commercial reprints: [Click here](#)

Terms of use : [Click here](#)



Parametric excitation-based inverse bending gait generation

Yuji Harata, Fumihiko Asano, Kouichi Taji and Yoji Uno

Robotica / Volume null / Issue 06 / October 2011, pp 831 - 841

DOI: 10.1017/S026357471100004X, Published online: 10 February 2011

Link to this article: http://journals.cambridge.org/abstract_S026357471100004X

How to cite this article:

Yuji Harata, Fumihiko Asano, Kouichi Taji and Yoji Uno (2011). Parametric excitation-based inverse bending gait generation. Robotica, null, pp 831-841 doi:10.1017/S026357471100004X

Request Permissions : [Click here](#)

Parametric excitation-based inverse bending gait generation

Yuji Harata^{†,*}, Fumihiko Asano[‡], Kouichi Taji[§] and Yoji Uno[§]

[†]*Division of Mechanical Systems and Applied Mechanics, Faculty of Engineering, Hiroshima University, 1-4-1, Kagamiyama, Higashi-Hiroshima, Hiroshima, 739-8527, Japan*

[‡]*School of Information Science, Japan Advanced Institute of Science and Technology, 1-1, Asahidai, Nomi, Ishikawa, 923-1292, Japan. E-mail: fasano@jaist.ac.jp*

[§]*Department of Mechanical Science and Engineering, Graduate School of Engineering, Nagoya University, Furo-cho, Chikusa, Nagoya, Aichi, 464-8603, Japan. E-mail: {taji,uno}@nuem.nagoya-u.ac.jp*

(Received in Final Form: January 10, 2011. First published online: February 10, 2011)

SUMMARY

In a gait generation method based on the parametric excitation principle, appropriate motion of the center of mass restores kinetic energy lost by heel strike. The motion is realized by bending and stretching a swing-leg regardless of bending direction. In this paper, we first show that inverse bending restores more mechanical energy than forward bending, and then propose a parametric excitation-based inverse bending gait for a kneed biped robot, which improves gait efficiency of parametric excitation walking.

KEYWORDS: Parametric excitation; Dynamic bipedal walking; Energy restoration; Forward bending; Inverse bending.

1. Introduction

When a biped robot walks, mechanical energy lost by heel strike at the ground is unavoidable, and hence, restoration of mechanical energy is a requisite for sustainable walking. In passive dynamic walking proposed by McGeer,¹ potential energy is transported to kinetic energy as walking down a slope. For sustainable walking on a level ground, several methods for restoration of mechanical energy were proposed, for example, energy tracking control by Goswami *et al.*,² virtual passive dynamic walking by Asano *et al.*³ and so on.

Parametric excitation, an example of which is a children's swing, is another approach to restore mechanical energy by appropriate up-and-down movement of the center of mass (COM). Asano *et al.*^{4,5} first applied parametric excitation principle to a biped robot with telescopic legs, which made the swing-leg mass up-and-down, and showed that the robot walked sustainably. Asano *et al.*⁶ also applied parametric excitation to a real machine. Harata *et al.*⁷ applied parametric excitation principle to a kneed biped robot. This being similar to telescopic leg, bending and stretching a swing-leg knee causes up-and-down motion of COM of swing-leg. They showed that mechanical energy was restored by bending and stretching a knee only, and hence, a biped robot walked sustainably without hip actuation.

In this paper, we focus on the fact that the movement of COM is realized regardless of bending direction, that is, bending of a swing-leg inversely with human knees also moves COM up-and-down. Here, the bending way shown in Fig. 1(a) is called forward bending walking, and the bending way shown in Fig. 1(b) is called inverse bending walking.

An example of inverse bending is an acrobot,⁸ which has a mechanism similar to the swing-leg of our biped robot. The acrobot has an actuator on the knee and the robot can be controlled to swing up, which needs to increase mechanical energy. The acrobot bends in inverse direction, which is a similar fashion of giant swing on a horizontal bar. From this fact, we consider that inverse bending is suitable for energy restoration, and hence, it improves gait efficiency for the parametric excitation walking.

In order to improve gait efficiency for the parametric excitation walking, we propose and study parametric excitation-based inverse bending walking. First, we show that inverse bending increases more mechanical energy than forward bending. Next, we propose parametric excitation-based inverse bending walking and show that a robot can walk sustainably. Then, we compare inverse bending with forward bending for our biped model, and show that inverse bending walking is more efficient than forward bending with respect to some performance indices, such as walking speed and specific resistance.

This paper is organized as follows. Section 2 explains a biped robot with semicircular feet. In Section 3, we present the difference of energy restoration between forward bending and inverse bending for a double pendulum. Section 4 is the main part of this paper, in which we propose a sustainable gait generation method for the inverse bending walking and compare parametric excitation-based inverse bending walking to forward bending walking with our biped model. In Section 5, the parametric study is carried out. Finally in Section 6, we conclude this paper.

2. Model of Planar Kneed Biped Robot with Semicircular Feet

Figure 2 illustrates the model of a biped robot discussed in this paper. The robot has five point masses, such that each leg has two masses and the rest one is at hip joint, and

* Corresponding author. E-mail: harata@hiroshima-u.ac.jp

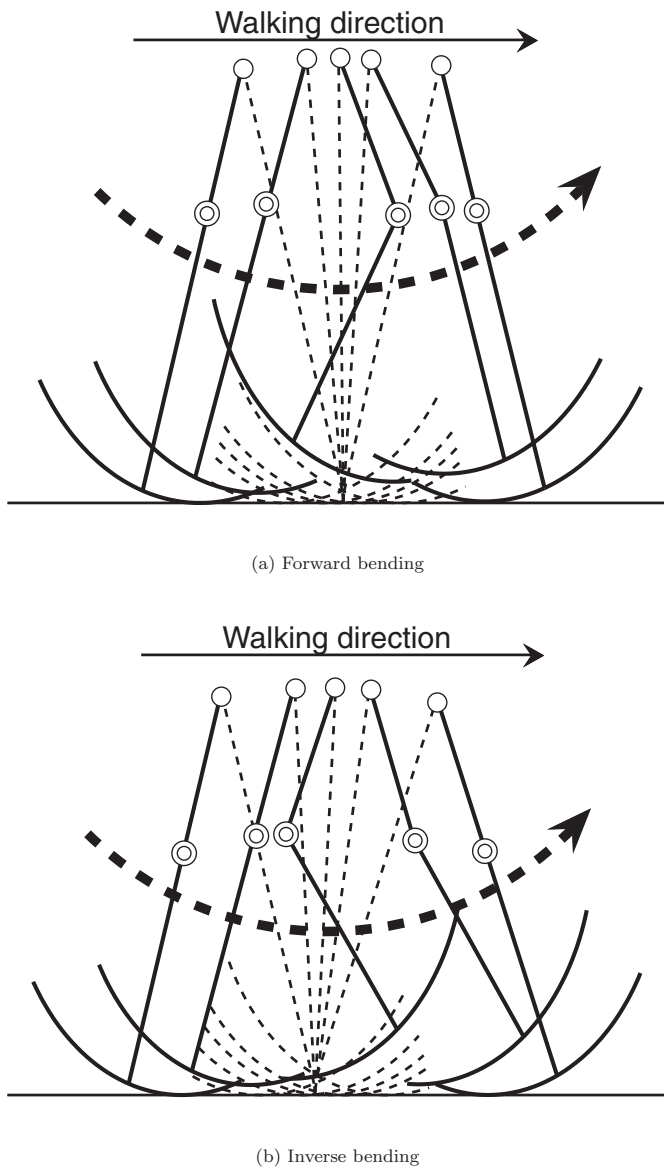


Fig. 1. Forward and inverse bending walking.

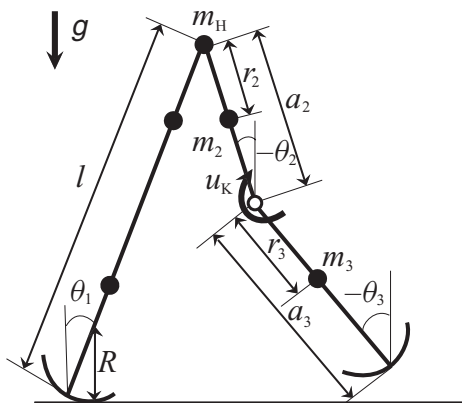


Fig. 2. Model of planar kneed biped robot with semicircular feet.

has semicircular feet whose centers are on each leg. Each leg has an actuated knee joint, but the support-leg is fixed in a straight posture (see Fig. 2). Therefore, the robot has three degrees of freedom, and three angles θ_1 , θ_2 , and θ_3 ,

as shown in Fig. 2, are taken as generalized coordinates. Each angle is taken in a clockwise direction from vertical upward.

The dynamic equation during single support phase takes the form

$$M(\theta)\ddot{\theta} + C(\theta, \dot{\theta})\dot{\theta} + g(\theta) = Su_K - J^T\lambda, \quad (1)$$

where $\theta = [\theta_1 \ \theta_2 \ \theta_3]^T$ is the generalized coordinate vector, $M \in \mathbb{R}^{3 \times 3}$ is the inertia matrix, $C \in \mathbb{R}^{3 \times 3}$ is the Coriolis force and the centrifugal force, and $g \in \mathbb{R}^{3 \times 1}$ is the gravity vector. The vector $J = [0 \ 1 \ -1]$ is the Jacobian derived from the constraint, $\theta_2 = \theta_3$, and $\lambda \in \mathbb{R}$ is knee-binding force. The control input vector Su_K in Eq. (1) is given by

$$Su_K = \begin{bmatrix} 0 \\ -1 \\ 1 \end{bmatrix} u_K, \quad (2)$$

where u_K is the input torque for a swing-leg knee.

In this robot, two types of collisions occur at a knee and at the ground. The robot gait consists of the following three phases:

- The first phase (single support phase I): The support-leg rotates around the contact point between the semicircular foot and ground, and the knee of the swing-leg is not fixed. In this phase, the knee-binding force λ equals to zero, and hence, knee angle of the swing-leg can be controlled by input torque.
- The second phase (single support phase II): The support-leg rotates around the contact point like the first phase, but the knee of the swing-leg is fixed in a straight posture by knee-binding force. When the first phase changes to the second phase, a completely inelastic collision is assumed to occur at the swing-leg knee.
- The third phase (double support phase): This phase occurs instantaneously, and then the role of the support-leg and that of the swing-leg are exchanged.

3. Effect of Bending Direction for a Double Pendulum

In this section, we show that inverse bending increases more energy than forward bending in a double pendulum.

3.1. Difference of energy restoration for a double pendulum

In the parametric excitation method, mechanical energy is restored by up-and-down motion of COM of a swing-leg, which is realized by bending and stretching a knee. However, regardless of bending direction, up-and-down motion can be realized, that is, COM also moves up-and-down as bending and stretching a knee in inverse direction with human movements. In this subsection, we analytically show the difference of energy restoration between bending directions. To do this, we use a double pendulum that has the similar mechanism of the swing-leg of the robot as shown in Fig. 2.

The dynamic equation of a double pendulum shown in Fig. 3 is given by

$$M_P(\theta)\ddot{\theta} + C_P(\theta, \dot{\theta})\dot{\theta} + G_P(\theta) = S_P u_P, \quad (3)$$

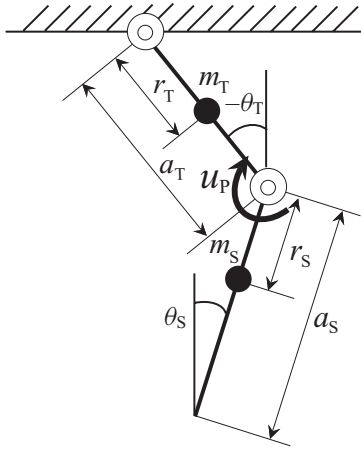


Fig. 3. Double pendulum.

where,

$$\mathbf{M}_P(\boldsymbol{\theta}) = \begin{bmatrix} M_{P11} & M_{P12} \\ M_{P21} & M_{P22} \end{bmatrix}, \quad (4a)$$

$$\mathbf{C}_P(\boldsymbol{\theta}, \dot{\boldsymbol{\theta}}) = \begin{bmatrix} m_S a_T r_S \dot{\theta}_S^2 \sin(\theta_T - \theta_S) \\ -m_S a_T r_S \dot{\theta}_T^2 \sin(\theta_T - \theta_S) \end{bmatrix}, \quad (4b)$$

$$\mathbf{G}_P(\boldsymbol{\theta}) = \begin{bmatrix} g(m_T r_T + m_S a_T) \sin \theta_T \\ g m_S r_S \sin \theta_S \end{bmatrix}, \quad (4c)$$

and

$$M_{P11} = m_T r_T^2 + m_S a_T^2, \quad (5a)$$

$$M_{P12} = m_S a_T r_S \cos(\theta_T - \theta_S), \quad (5b)$$

$$M_{P21} = m_S a_T r_S \cos(\theta_T - \theta_S), \quad (5c)$$

$$M_{P22} = m_S r_S^2. \quad (5d)$$

We give a reference trajectory h for the knee joint angle. In the same way as given in [7], the input torque u_P for the intermediate joint angle is designed by the partial feedback linearization method so as to track the reference trajectory h , such as

$$u_P = \frac{Z_P}{K_P}, \quad (6)$$

where K_P and Z_P are defined by

$$K_P = [0 \quad 1] (\mathbf{M}_P \mathbf{L}_P)^{-1} \mathbf{S}_P, \quad (7)$$

$$Z_P = [0 \quad 1] (\mathbf{M}_P \mathbf{L}_P)^{-1} \left(\mathbf{M}_P \begin{bmatrix} 0 \\ -\ddot{h} \end{bmatrix} + \mathbf{C}_P + \mathbf{G}_P \right),$$

respectively, and matrices \mathbf{L}_P and \mathbf{S}_P are given by

$$\mathbf{L}_P = \begin{bmatrix} 1 & 0 \\ 1 & -1 \end{bmatrix}, \quad \mathbf{S}_P = \begin{bmatrix} 1 \\ -1 \end{bmatrix}. \quad (8)$$

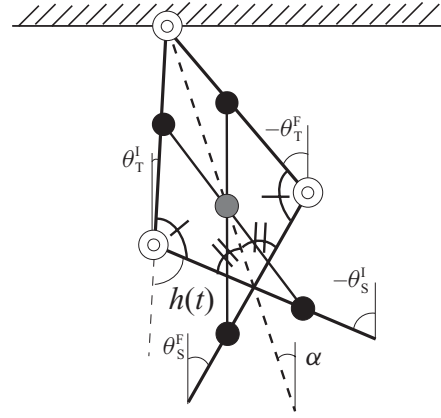


Fig. 4. Symmetry of forward bending and inverse bending.

By using this input, Eq. (3) is reduced to

$$\ddot{\theta}_T - \ddot{\theta}_S = \ddot{h}. \quad (9)$$

Equation (9) means that if the initial condition satisfies $\theta_T(0) - \theta_S(0) = h(0)$ and $\dot{\theta}_T(0) - \dot{\theta}_S(0) = \dot{h}(0)$, the relative angle tracks the reference trajectory h .

For the up-and-down motion of COM, there is no difference between inverse bending and forward bending except for bending direction, and hence, we assume that $h^F(t) = -h^I(t)$, whose superscripts “F” and “I” correspond to forward bending and inverse bending, respectively. We suppose that the following relations hold:

$$\begin{aligned} \cos(\theta_T^F - \theta_S^F) &= \cos(h^F) = \cos(\theta_T^I - \theta_S^I), \\ \sin(\theta_T^F - \theta_S^F) &= \sin(h^F) = -\sin(\theta_T^I - \theta_S^I), \end{aligned} \quad (10)$$

$$\mathbf{M}_P^F(\boldsymbol{\theta}) = \mathbf{M}_P^I(\boldsymbol{\theta}).$$

For simplicity, we consider only one cycle of the pendulum in which the initial states of forward and inverse bending are the same. In addition, we assume the followings:

- Assumption 1 : Oscillation of the pendulum is sufficiently small, i.e., $|\theta_T| \ll 1$ and $|\theta_S| \ll 1$.
- Assumption 2 : Inverse bending and forward bending are symmetric as shown in Fig. 4, i.e.,

$$\frac{\theta_T^F + \theta_T^I}{2} = \frac{\theta_S^F + \theta_S^I}{2} = \alpha, \quad (11)$$

where α is the angle of the line connecting the support point and COM of the pendulum from the vertical line (see Fig. 4).

From the Assumption 1, \mathbf{C}_P and \mathbf{G}_P in Eqs. (4b) and (4c) are rewritten by eliminating the higher order terms as

$$\begin{aligned} \mathbf{C}_P &= \mathbf{0}_{2 \times 1}, \\ \mathbf{G}_P &= \begin{bmatrix} g(m_T r_T + m_S a_T) \theta_T \\ g m_S r_S \theta_S \end{bmatrix}. \end{aligned}$$

The input power for the pendulum given by

$$\dot{E} = \dot{\theta}^T S_P u_P, \quad (12)$$

is rewritten as

$$\dot{E} = \dot{\theta}^T S_P u_P = (\dot{\theta}_T - \dot{\theta}_S) u_P = \dot{h}^F K_P^{-1} Z_P$$

by Eq. (6). We define the row vector \mathbf{W} as $\mathbf{W} := K_P^{-1} [0 \quad 1] (\mathbf{M}_P \mathbf{L}_P)^{-1}$, then

$$\mathbf{W} = \frac{1}{m_T r_T^2 + m_S (a_T + m_S r_S)^2} X [m_S r_S^2 + m_S a_T r_S - (m_S a_T r_S + m_T r_T^2 + m_S a_T^2)].$$

Therefore, the input powers of forward bending and inverse bending are given by

$$\begin{aligned} \dot{E}^F &= \dot{h}^F \mathbf{W} \left(\mathbf{M}_P \begin{bmatrix} 0 \\ -\dot{h}^F \end{bmatrix} + \mathbf{G}_P^F \right), \\ \dot{E}^I &= -\dot{h}^F \mathbf{W} \left(\mathbf{M}_P \begin{bmatrix} 0 \\ \dot{h}^F \end{bmatrix} + \mathbf{G}_P^I \right), \end{aligned}$$

respectively. The difference of input power between forward bending and inverse bending is calculated as

$$\dot{E}^I - \dot{E}^F = -\dot{h}^F \mathbf{W} (\mathbf{G}_P^F + \mathbf{G}_P^I). \quad (13)$$

Under Assumption 2, Eq. (13) is rewritten as

$$\dot{E}^I - \dot{E}^F = -2\dot{h}^F \alpha g \frac{m_S m_T r_S r_T (r_S + a_T - r_T)}{m_T r_T^2 + m_S (a_T + r_S)^2}. \quad (14)$$

Let's consider the motion of the pendulum be split into two parts at the vertical line. We suppose that the knee is bent until COM passes through the vertical line (first half) and it is stretched after that (second half). Then, $\alpha > 0$ and $\dot{h}^F < 0$ hold in the first half, and $\alpha < 0$ and $\dot{h}^F > 0$ hold in the second half. This gives the relation $\alpha \dot{h}^F < 0$, or equivalently, $\dot{E}^I - \dot{E}^F > 0$. Since the energy restoration of one cycle is given by

$$\Delta E = \int_0^T \dot{E} dt, \quad (15)$$

we conclude that

$$\Delta E^F < \Delta E^I. \quad (16)$$

This shows that inverse bending restores more mechanical energy than forward bending in the case of infinitesimal oscillation.

3.2. Numerical simulation

In this subsection, we compare the energy restoration of inverse bending with that of forward bending by numerical simulation. Parameters of the double pendulum are shown in Table I. Figure 5 presents the optimal trajectory, A \rightarrow

Table I. Physical parameters of the double pendulum.

r_T	0.20 m	r_S	0.30 m
m_T	1.0 kg	m_S	4.0 kg
a_T	0.40 m	a_S	0.60 m

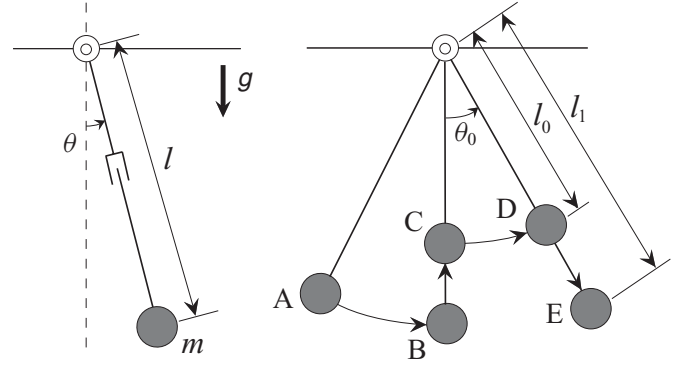


Fig. 5. Optimal trajectory of pendulum for parametric excitation.

B \rightarrow C \rightarrow D \rightarrow E, for a pendulum, given by Lavrovskii and Formalskii,⁹ along which increase of mechanical energy is maximized, with supposition that the length, l , of the pendulum is changed instantaneously. However, since the length cannot be changed instantaneously, a reference trajectory close to the optimal trajectory is chosen. We give the reference trajectory of an intermediate joint as

$$h(t) = (\theta_T - \theta_S)_d = \begin{cases} \beta A_m \sin^3 \left(\frac{\pi}{T_{\text{set}}} t \right) & (t \leq T_{\text{set}}) \\ 0 & (t > T_{\text{set}}) \end{cases}, \quad (17)$$

where A_m is the maximum bending angle, and T_{set} is the settling time. Parameter $\beta = \pm 1$ determines bending direction, i.e., forward bending as $\beta = -1$ and inverse bending direction as $\beta = 1$. The time parameter t means a relative time from the instance of $\theta_T = \theta_S = 0$ with $\theta_T = \theta_S > 0$, that is, t is reset to be zero at the instance. In the trajectory Eq. (17), the pendulum is bent from $t = 0$ to $t = T_{\text{set}}/2$ and stretched from $t = T_{\text{set}}/2$ to $t = T_{\text{set}}$. If the settling time equals to the half period of one cycle, the motion of the pendulum satisfies the assumption that the knee is bent in the first half and stretched in the second half. In addition, the angular velocity and the acceleration of reference trajectory are zero as $t = 0$ and $t = T_{\text{set}}$.

Figure 6 illustrates the mechanical energy of the simulation result in the case that $A_m = 1.5$ rad, $T_{\text{set}} = 0.9$ s, and initial condition $\alpha = 0.4$ rad. In Fig. 6, the solid line shows the forward bending result and the dashed line shows the inverse bending result. Mechanical energy increases when the pendulum is bent from $t = 0$ to $t = T_{\text{set}}/2$ because potential energy increases as COM up. On the other hand, the energy decreases when the pendulum is stretched from $t = T_{\text{set}}/2$ to $t = T_{\text{set}}$ because potential energy decreases as COM down. After that, the pendulum is fixed to a straight posture until the time parameter is reset, and hence, mechanical energy is constant. From Fig. 6 it is observed that inverse bending restores more mechanical energy than forward bending.

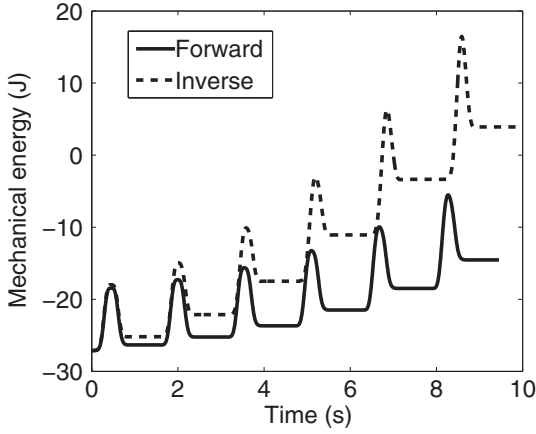


Fig. 6. Difference of energy restoration between forward bending and inverse bending.

As seen above, inverse bending is suitable for energy restoration, and hence, we expect that inverse bending walking is more efficient than forward bending walking.

This analysis has nothing but theoretical meaning because there is significant difference between a pendulum and the biped robots. The hip joint of a biped robot is movable, while the supporting point of a pendulum is fixed at a ceiling. In spite of this, we will generate inverse bending walking with the expectation of increasing more kinematic energy.

4. Inverse Bending Parametric Excitation Walking

In this section, we design the control input of the biped robot and show the numerical simulation results. In addition, we compare the inverse bending walking with the forward bending walking.

4.1. Control input design

In this subsection, the control input design for the kneed biped robot shown in Fig. 2 is explained.

A reference trajectory for the relative knee-joint angle is given as

$$\begin{aligned}
 (\theta_2 - \theta_3)_d &= f(t) \\
 &= \begin{cases} \beta A_m \sin^3 \left(\frac{\pi}{T_{\text{set}} - \delta} (t - \delta) \right) & (\delta \leq t \leq T_{\text{set}}) \\ 0 & (\text{otherwise}), \end{cases} \quad (18)
 \end{aligned}$$

where $\delta > 0$ is the beginning time of bending, A_m is the maximum bending angle, and T_{set} is the settling time that defines the end of stretching. The parameter $\beta = \pm 1$ is used to indicate bending direction as explained in the previous section. In this trajectory, the angular velocity equals to zero at the beginning of bending and the end of stretching, and hence, the collision at knee is negligible. The time parameter, t , means a relative time from the beginning of the first phase, that is, t is reset to be zero at just after the third phase: the reason why introduction of parameter δ is illustrated in Fig. 7, where the dashed-dotted line is the

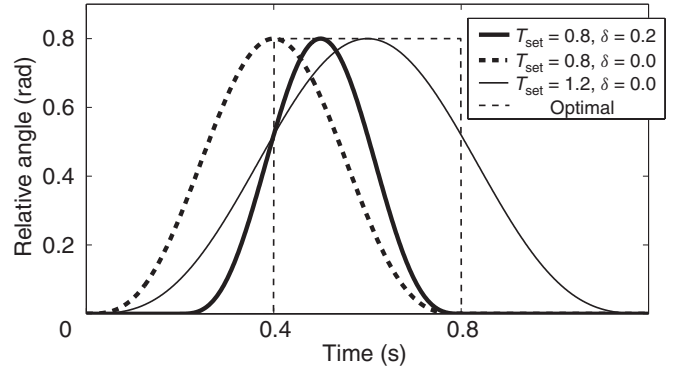


Fig. 7. Reference trajectories for knee angle.

optimal trajectory of the telescopic pendulum as shown in Fig. 5, the dot-line is the case of $\delta = 0$ s and the solid line is the case of $\delta = 0.2$ s. It is shown in Fig. 7 that the reference trajectory (solid line) approaches the optimal trajectory in the case $\delta = 0.2$ s, and hence, it is expected to restore more mechanical energy than those without δ .

In the rest of this subsection, we design control input to track the reference trajectory given by Eq. (18). Let's define $\mathbf{x} = [\theta_1 \quad \theta_2 \quad \theta_2 - \theta_3 - f]^T$, and let $\boldsymbol{\theta}$ be rewritten by

$$\boldsymbol{\theta} = \mathbf{L}\mathbf{x} + \mathbf{N} := \begin{bmatrix} 1 & 0 & 0 \\ 0 & 1 & 0 \\ 0 & 1 & -1 \end{bmatrix} \mathbf{x} + \begin{bmatrix} 0 \\ 0 \\ -f \end{bmatrix}. \quad (19)$$

Since $\dot{\boldsymbol{\theta}}$ and $\ddot{\boldsymbol{\theta}}$ are

$$\dot{\boldsymbol{\theta}} = \mathbf{L}\dot{\mathbf{x}} + \dot{\mathbf{N}} \quad \text{and} \quad \ddot{\boldsymbol{\theta}} = \mathbf{L}\ddot{\mathbf{x}} + \ddot{\mathbf{N}}, \quad (20)$$

the dynamic Eq. (1) in the first phase is redefined as

$$\mathbf{M}\mathbf{L}\ddot{\mathbf{x}} + \mathbf{M}\dot{\mathbf{N}} + \mathbf{C}\mathbf{L}\dot{\mathbf{x}} + \mathbf{C}\dot{\mathbf{N}} + \mathbf{g} = \mathbf{S}u_K. \quad (21)$$

Let's define \mathbf{K} as

$$\mathbf{K} = [0 \quad 0 \quad 1] \mathbf{L}^{-1} [\mathbf{M}^{-1} \mathbf{S}], \quad (22)$$

and select the knee torque u_K as

$$u_K = \frac{Z}{K}, \quad (23)$$

where Z is defined by

$$Z = [0 \quad 0 \quad 1] \mathbf{L}^{-1} \mathbf{M}^{-1} (\mathbf{M}\dot{\mathbf{N}} + \mathbf{C}\mathbf{L}\dot{\mathbf{x}} + \mathbf{C}\dot{\mathbf{N}} + \mathbf{g}). \quad (24)$$

Using Eqs. (22)–(24), the dynamic Eq. (21) reduces to

$$\ddot{\theta}_2 - \ddot{\theta}_3 = \ddot{f}. \quad (25)$$

By integrating this equation twice, we obtain

$$\begin{aligned}
 (\theta_2(t) - \theta_3(t)) - (\theta_2(0) - \theta_3(0)) - (\dot{\theta}_2(0) - \dot{\theta}_3(0))t \\
 = f(t) - f(0) - \dot{f}(0)t. \quad (26)
 \end{aligned}$$

Table II. Physical parameters of the kneed biped robot.

r_2	0.20 m		
r_3	0.30 m	m_2	1.0 kg
a_2	0.40 m	m_3	4.0 kg
a_3	0.60 m	m_H	5.5 kg
l	1.0 m		
R	0.575 m		

If initial states equal to the initial states of the reference trajectory, i.e., $\theta_2(0) - \theta_3(0) = \dot{f}(0)$ and $\theta_2(0) - \theta_3(0) = f(0)$, then Eq. (26) can be rewritten as

$$\theta_2(t) - \theta_3(t) = f(t). \quad (27)$$

Therefore, the input u_K given by Eq. (23) is shown to track the reference trajectory $f(t)$.

4.2. Numerical simulation results

We present the simulation results of parametric excitation-based inverse bending walking for the biped robot (Fig. 2), whose parameters are shown in Table II. We note that in this model the shin mass is four times larger than the thigh mass unlike in humans. This is because energy restoration based on the principle of parametric excitation needs up-and-down motion of COM of the swing-leg, i.e., if the shin mass is small, bending the knee makes little up-and-down motion effect of COM, and hence, mechanical energy is not restored sufficiently.

In this simulation, we show the results after the biped robot walks more than 100 steps. This is because a steady gait for the given reference trajectory is, in general, difficult to obtain analytically, and hence, we regard that the biped gait converges to period one walking when the biped robot walks 100 steps.

Figure 8 illustrates the simulation results between 105 s and 108 s after the start of simulation, whose initial conditions are $[\theta^T, \dot{\theta}^T] = [-0.21, 0.21, 0.21, 1.0, 0.90615, 0.90615]$. Here the parameters of the reference trajectory are set as the maximum bending angle $A_m = 0.8$ rad, the settling time $T_{\text{set}} = 0.8$ s, and the beginning time $\delta = 0.2$ s. Figures 8(a)–(d) are angular position, angular velocity, mechanical energy, and knee torque, u_K , respectively, and Fig. 8(e) is foot clearance, which is the height between the bottom of the swing-leg and the ground level. From Fig. 8(a), $\theta_2 - \theta_3$ is found to be always larger than or equal to 0, that is, the knee is bent in inverse direction. From Fig. 8(c), energy dissipation of the collision at the knee is seldom observed, while energy dissipation by heel strike is relatively large. That is why $\dot{\theta}_2 - \dot{\theta}_3$ is almost zero just before knee impact, according to the reference trajectory defined by Eq. (18). Figure 8(e) shows that foot clearance is positive except for the third phase (double support phase), and hence, the biped avoids scuffing the ground. In summary, it is found from the figures that the robot walks sustainably with inverse bending. Figure 9 shows stick diagram of one step of gait. Figure 10 illustrates relative position between COM of the swing-leg and hip joint. In Fig. 10, the solid line shows the simulation result and the dashed line shows the optimal trajectory for the

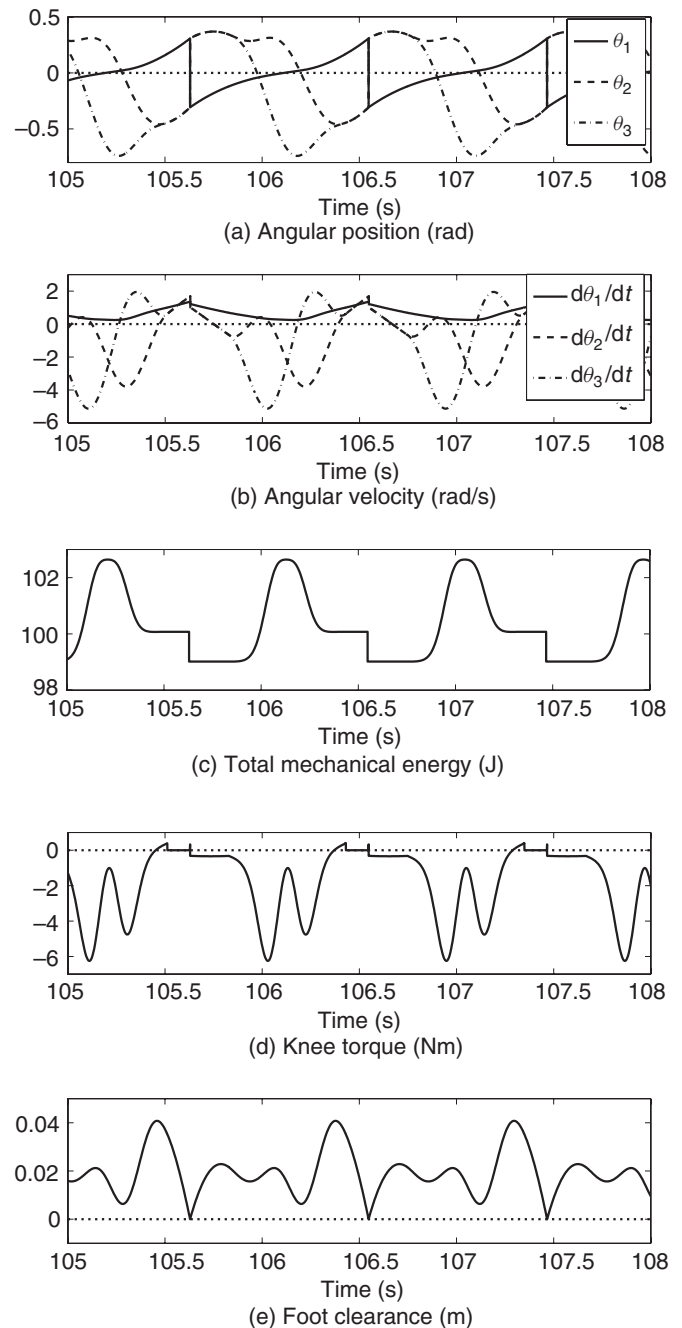


Fig. 8. Simulation results for inverse bending walking.

telescopic pendulum (shown in Fig. 5). The arrows indicate the motion direction, the white circle shows the position at the lift leg off, and the black circle shows the position at heel strike. COM first moves backward, then moves forward and up by bending the knee, and moves down by stretching the knee. After stretching the knee to a straight posture, heel strike occurs. The figure shows that COM moves smoothly along the optimal trajectory of the pendulum.

4.3. Comparison between inverse bending walking and forward bending walking

In this subsection, we compare inverse bending walking and forward bending walking with respect to step period, walking speed, and specific resistance (SR). Specific resistance is the

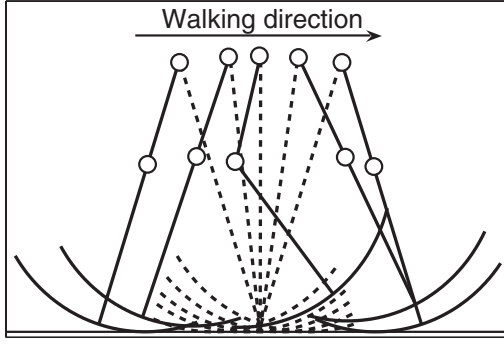


Fig. 9. Stick diagram of inverse bending walking.

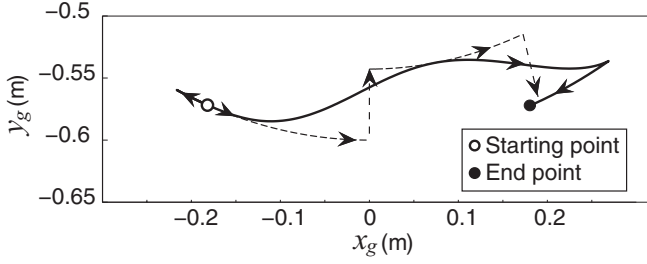


Fig. 10. Position of COM of swing-leg.

nondimensional value defined as

$$SR = \frac{\int_{0^+}^{T^-} |u_K(\dot{\theta}_2 - \dot{\theta}_3)| dt / T}{M_g g \bar{V}}, \quad (28)$$

where 0^+ and T^- represent the time just after and just before heel strike, respectively, M_g is the total mass of a robot, and \bar{V} is an average walking speed of one cycle. The denominator of Eq. (28) represents walking distance and the numerator represents the sum of absolute input energy. This means that SR is energy consumption when a biped robot walks a distance, and hence, the walking is more efficient as the SR is smaller.

First, inverse bending walking is compared with forward bending walking for the same reference trajectory. The parameters are set as $R = 0.6$ m, $a_2 = 0.35$ m, $r_2 = 0.175$ m, $a_3 = 0.75$ m, $r_a = 0.375$ m, $A_m = 1.2$ rad, $T_{set} = 0.75$ s, and $\delta = 0.2$ s. In these parameters, bipedal walking converges to period one walking for both inverse bending walking and forward bending walking. Table III shows the simulation results. In this table, foot clearance represents the minimum value of foot clearance during one cycle. This table shows that inverse bending walking is better with respect to walking speed and SR. In both cases, the robot avoids scuffing the ground.

Next, inverse bending walking is compared with forward bending walking at almost the same walking speed. In the parametric excitation method, mechanical energy increases when bending a swing-leg and decreases when stretching. When the energy variation caused by bending and stretching the swing-leg becomes large, the numerator of Eq. (28) increases. Therefore, in the case of same walking speed, SR is small if energy variation is small. Figure 11 illustrates the

Table III. Gait descriptors of inverse bending walking and forward bending walking.

	Inverse bending	Forward bending
Step period	0.91 s	0.85 s
Walking speed	0.83 m/s	0.67 m/s
Specific resistance	0.11	0.15
Foot clearance	0.019 m	0.0031 m

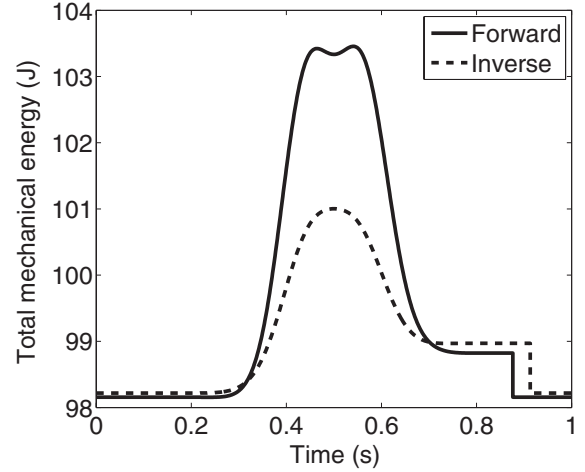


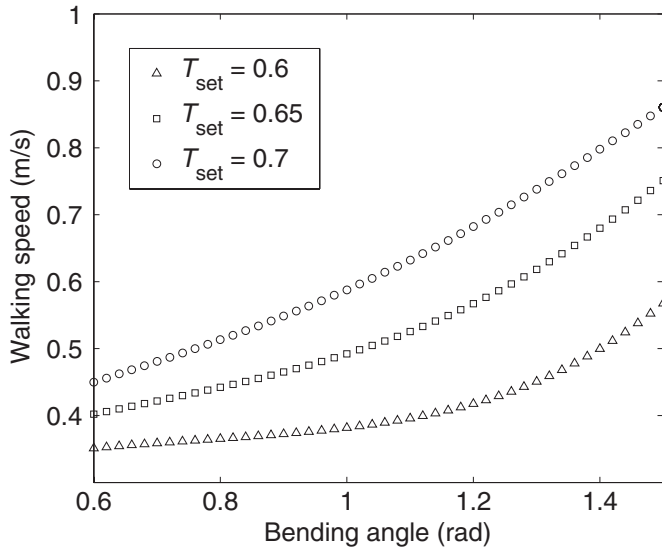
Fig. 11. Cyclic variation of total mechanical energy.

mechanical energy in forward bending walking and inverse bending walking. In Fig. 11, the dashed line shows inverse bending walking and the solid line shows forward bending walking for walking speed of about 0.618 m/s. From Fig. 11, it is observed that mechanical energy of inverse bending walking increases from 98 to 101 J and decreases from 101 to 99 J. On the other hand, mechanical energy of forward bending walking increases from 98 to 103.5 J and decreases from 103.5 to 99 J. Then the energy variation of inverse bending walking is 5 J, while that of forward bending walking is 10 J. This result shows that inverse bending walking is more efficient than forward bending walking.

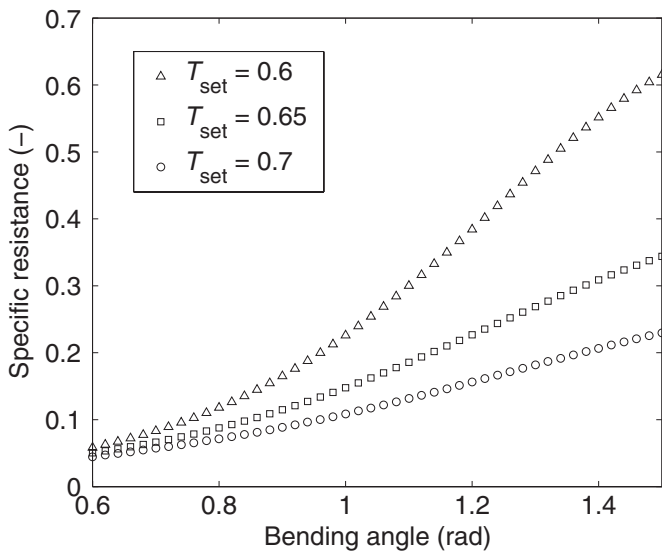
5. Effect of Parameters

In this section, we study the effect of the reference trajectory parameters, the physical parameters, and the initial conditions on walking performance. In our model, the shin mass has been four times larger than the thigh mass to sufficiently restore the mechanical energy. In addition, our model has the large feet to decrease energy dissipation by heel strike.¹⁰ We showed in the previous section that inverse bending restores more mechanical energy than forward bending. Therefore, in the parametric study for the biped robot we show that the shin mass and the foot radius can be decreased. On the other hand, the parametric study for the reference trajectory is carried out to clarify the effect of the reference trajectory and this leads to determine the efficient parameters of the trajectory. The effect of the initial condition is studied to evaluate the stability of the gait.

We perform numerical simulation in changing one of the parameters, such as the maximum bending angle, the settling



(a) Walking speed



(b) Specific resistance

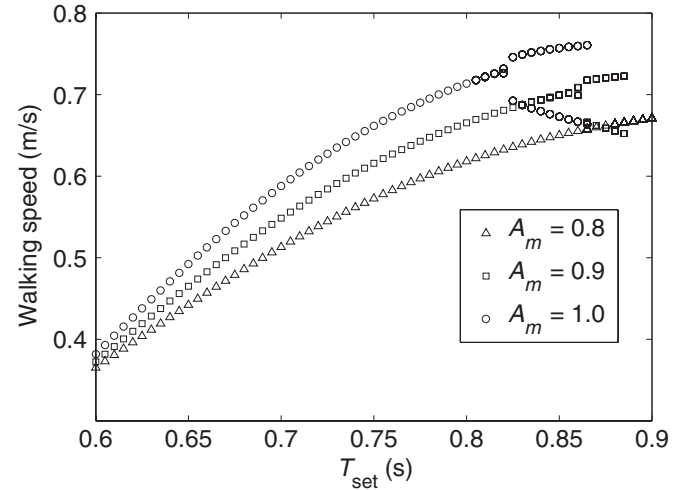
Fig. 12. Effect of bending angle.

time, the beginning time, the shin mass, the foot radius, and the initial condition. Throughout the numerical simulation in this section, physical parameters of robot are set as those shown in Table II unless otherwise stated. In the simulation, we illustrate only the results in which we can generate sustainable gait. However, we ignore the possibility that the biped feet scuff the ground.

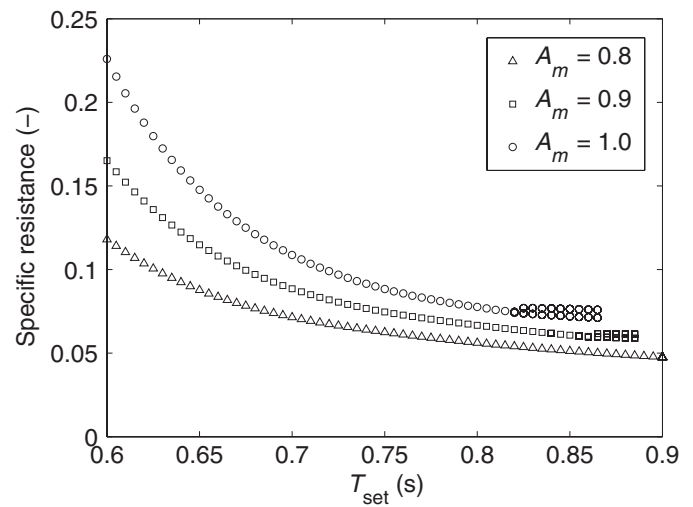
5.1. Parameters of reference trajectory

In this subsection, gait performance is evaluated as changing the parameters of the reference trajectory.

First, we fix $T_{set} = 0.60, 0.65, 0.70$ s and $\delta = 0.2$ s and change the bending angle, A_m from 1.0 rad to 1.5 rad. Walking speed and SR are evaluated for each bending angle. Figure 12 shows the simulation results. In Fig. 12, the triangles denote the results of the settling time $T_{set} = 0.6$ s, the squares denote the results of $T_{set} = 0.65$ s, and the circles denote the results of $T_{set} = 0.7$ s. From Fig. 12, it is observed



(a) Walking speed

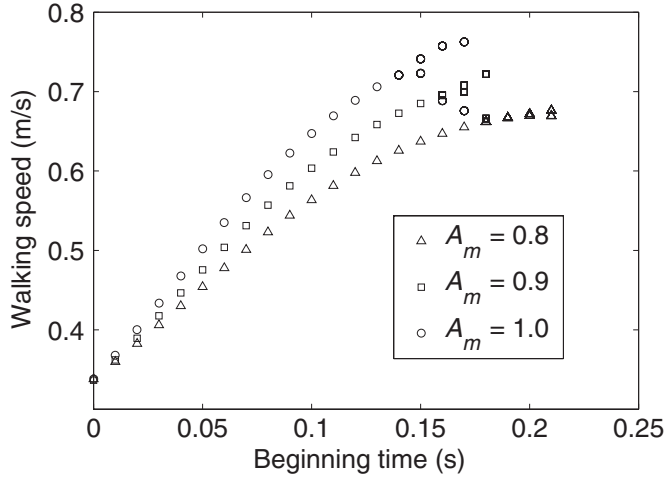


(b) Specific resistance

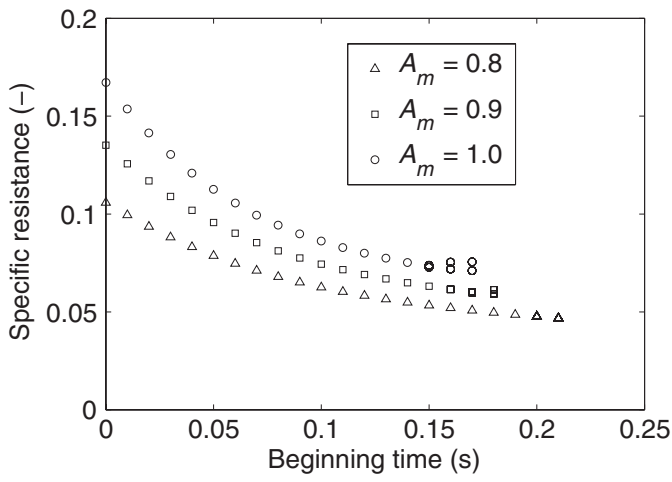
Fig. 13. Effect of settling time.

that walking speed and SR become large as the bending angle, A_m , increases. This is because when the bending angle becomes large, more mechanical energy is restored, and hence, walking speed becomes large. On the other hand, input torque and angular velocity of the knee also become large. The simulation results also show that the walking speed is larger and the SR is smaller.

Next, we fix $A_m = 0.8, 0.9, 1.0$ rad and $\delta = 0.2$ s and change the settling time, T_{set} from 0.6 s to 0.9 s. Figure 13 shows the simulation result. In Fig. 13, the triangles denote the results of the bending angle $A_m = 0.8$ rad, the squares denote the results of $A_m = 0.9$ rad, and the circles denote the results of $A_m = 1.0$ rad. It is observed from Fig. 13 that walking speed is larger and SR is smaller as the settling time T_{set} increases. In addition, period doubling bifurcation occurs when $T_{set} \geq 0.85$ s and $A_m = 0.9$ rad, and $T_{set} \geq 0.815$ s and $A_m = 1.0$ rad. This indicates that more mechanical energy is restored when T_{set} and A_m are larger. When the settling time is large, angular velocity of the swing-leg is small. However, there is an upper bound of the settling time, because we assume that heel strike occurs after the knee is stretched to



(a) Walking speed



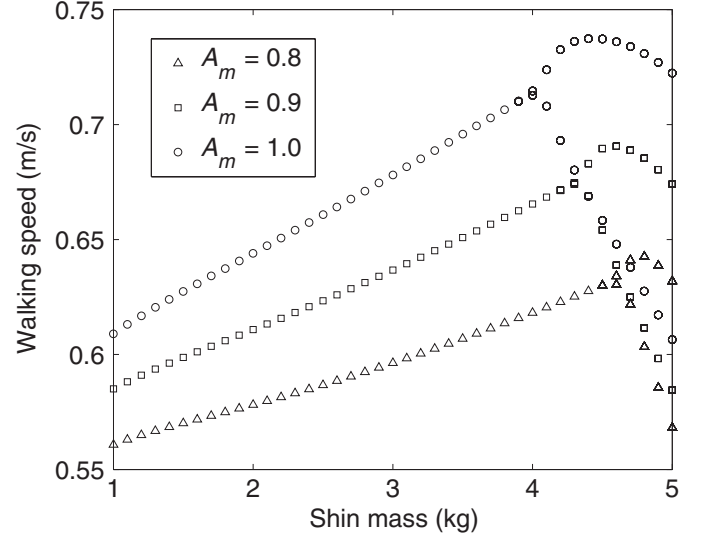
(b) Specific resistance

Fig. 14. Effect of beginning time.

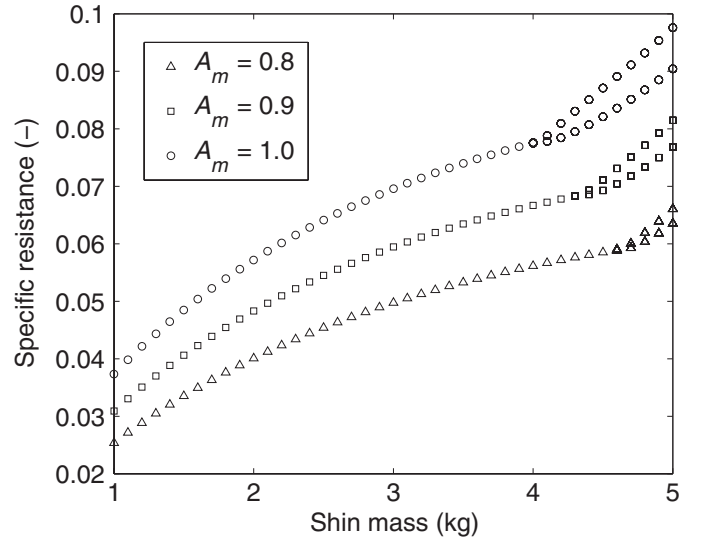
a straight posture. If the setting time is too large, heel strike may occur before the swing-leg is stretched to a straight posture, for example, $T_{\text{set}} \leq 0.885$ s when $A_m = 0.9$ rad and $T_{\text{set}} \leq 0.865$ s when $A_m = 1.0$ rad.

Finally, we fix $A_m = 0.8, 0.9, 1.0$ rad and $T_{\text{set}} - \delta = 0.7$ s and change the beginning time, δ , from 0.0 to 0.4 s. Figure 14 shows the simulation results. In Fig. 14, the triangles denote the results of the bending angle $A_m = 0.8$ rad, the squares denote the results of $A_m = 0.9$ rad, and the circles denote the results of $A_m = 1.0$ rad. Figure 14 shows that walking speed is larger and SR is smaller as the beginning time, δ , increases. Period doubling bifurcation also occurs when $\delta \geq 0.19$ s and $A_m = 0.8$ rad, $\delta \geq 0.15$ s, and $A_m = 0.9$ rad, and $\delta \geq 0.14$ s and $A_m = 1.0$ rad. There is also an upper bound of the beginning time, for example, $\delta \leq 0.21$ s when $A_m = 0.8$ rad, $\delta \leq 0.18$ s when $A_m = 0.9$ rad, and $\delta \leq 0.17$ s when $A_m = 1.0$ rad.

These results indicate that to increase the walking speed all the bending angles, the settling time, and the beginning time δ are made larger. But the effect of these three parameters is slightly different. If A_m increases, angular velocity of the knee becomes large. On the other hand, if



(a) Walking speed



(b) Specific resistance

Fig. 15. Effect of shin mass.

T_{set} and δ increase, the gait becomes more efficient with the angular velocity fixed; especially when T_{set} increases, angular velocity becomes small. This is because angular velocity of the knee joint is proportional to the bending angle and is inversely proportional to the settling time (see Eq. (18)). Small angular velocity of the knee joint is desirable in view of maximum actuator torque, and hence, increase of T_{set} is most acceptable for realizing high-speed gait, although there is an upper bound.

5.2. Physical parameters

In this subsection, we change the physical parameters and evaluate gait performance.

We first fix $A_m = 0.8, 0.9, 1.0$ rad, $T_{\text{set}} = 0.8$ s and $\delta = 0.2$ s, and change the shin mass, m_3 , from 5.0 kg to 1.0 kg. Figure 15 shows the simulation results. In Fig. 15, the triangles denote the results of the bending angle $A_m = 0.8$ rad, the squares denote the results of $A_m = 0.9$ rad, and the circles denote the results of $A_m = 1.0$ rad. Figure 15 shows

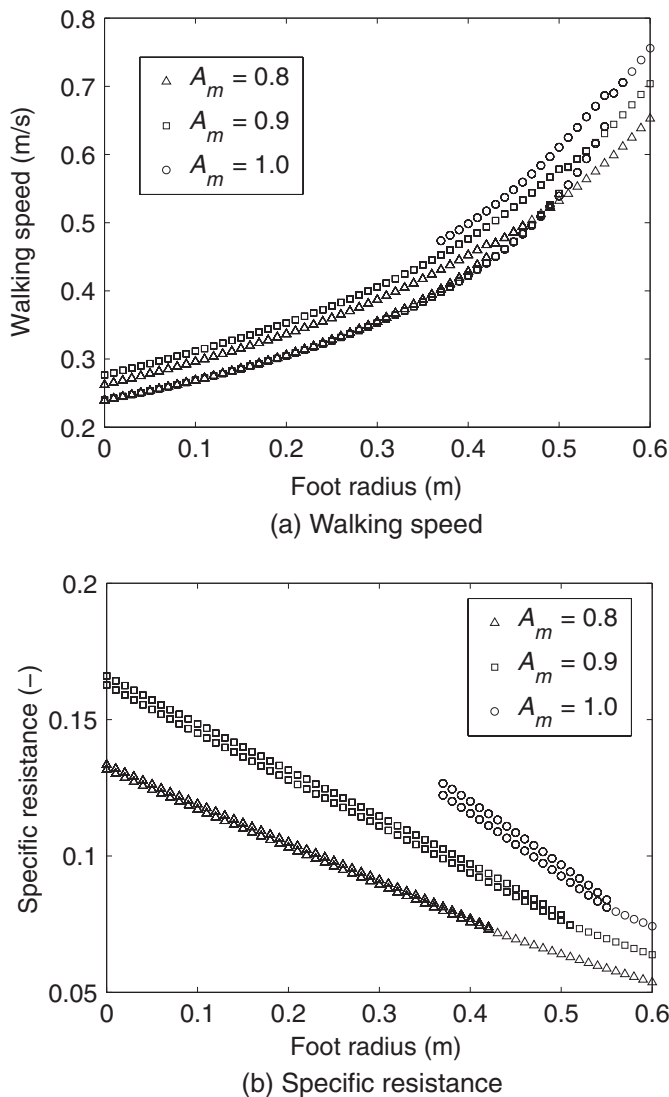


Fig. 16. Effect of foot radius.

that walking speed and SR are larger as the shin mass, m_3 , increases. Period doubling bifurcation occurs when $m_3 \geq 4.5$ kg and $A_m = 0.8$ rad, $m_3 \geq 4.2$ kg and $A_m = 0.9$ rad, and $m_3 \geq 3.9$ kg and $A_m = 1.0$ rad. This is because input torque and energy restoration becomes large when the shin mass increases.

Next, we fix $A_m = 0.8, 0.9, 1.0$ rad, $T_{\text{set}} = 0.8$ s, and $\delta = 0.2$ s and change the foot radius, R , from 0.6 to 0.0 m. Figure 16 shows the simulation results. In Fig. 16, the triangles denote the results of the bending angle $A_m = 0.8$ rad, the squares denote the results of $A_m = 0.9$ rad, and the circles denote the results of $A_m = 1.0$ rad. Figure 16 shows that the biped robot cannot walk when $A_m = 1.0$ rad and $R \leq 0.37$ m. Period doubling bifurcation occurs when $R \leq 0.43$ m and $A_m = 0.8$ rad, $R \geq 0.51$ m and $A_m = 0.9$ rad, and $R \geq 0.56$ m and $A_m = 1.0$ rad.

The above two results indicate that the both shin mass and foot can be made small. Then, we search appropriate parameters to generate sustainable gait with *point foot*. Here, we set $A_m = 0.8$ rad, $T_{\text{set}} = 0.8$ s, $\delta = 0.2$ s, $R = 0$ m, and $m_3 = 2.5$ kg. Simulation result illustrated in Fig. 17 is one step after the gait converges to period one walking.

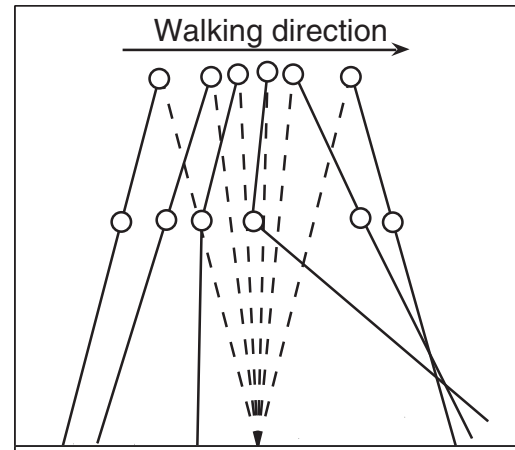


Fig. 17. Stick diagram in the case of point foot.

Figure 17 shows that the biped robot with point foot can walk sustainably.

5.3. Basin of attraction

In this subsection, we calculate the basin of attraction. To do this, we consider the sustainable gait, for which the target control input corresponds to $A_m = 0.8$ rad, $T_{\text{set}} = 0.8$ s, and $\delta = 0.2$ s, and we simulate the motion from the several initial conditions. Our robot has three degrees of freedom for initial conditions, i.e., the support-leg angle, the support-leg angular velocity, and the swing-leg angular velocity. We perform the simulation for the initial conditions, such that the support-leg angle θ_1 changes from 0.1 to 0.4 rad, and the angular velocities $\dot{\theta}_1$ and $\dot{\theta}_2$ change from 0.0 to 2.0 rad/s. We regard an initial condition belongs to the basin of attraction when the biped robot walks 100 steps successfully.

Simulation results of the basin of attraction are shown in Fig. 18, which depicts three slices of two-dimensional figures. The axes represent the initial conditions of the system. Figures 18(a)–(c) are the results for $\theta_1 = -0.284$ rad, $\dot{\theta}_2 = 0.969$ rad/s, and $\dot{\theta}_1 = 1.137$ rad/s, respectively. In these figures, the circles indicate the initial conditions from which the robot walks sustainably and the initial condition converges to the fixed point indicated by the star, $[\theta_1 \theta_2 \theta_3 \dot{\theta}_1 \dot{\theta}_2 \dot{\theta}_3] = [-0.284 \ 0.284 \ 0.284 \ 1.137 \ 0.969 \ 0.969]$.

In order to evaluate the basin of attraction, we calculate the minimum relative error of the attraction from the fixed point for each slice. The relative errors in Figs. 18(a)–(c) are 2.3%, 1.22%, and 13.76%, respectively.

6. Conclusion and Future Work

In this paper, we proposed parametric excitation-based inverse bending walking. First, we focused on the restoration of energy by bending and stretching a swing-leg. We showed by a double pendulum that inverse bending was more suitable for energy restoration than forward bending by linear analysis and numerical simulation. Then, we generated inverse bending walking with only knee torque like parametric excitation walking. We also showed that inverse bending walking was more efficient than forward bending walking. The parametric study showed that the effects of the

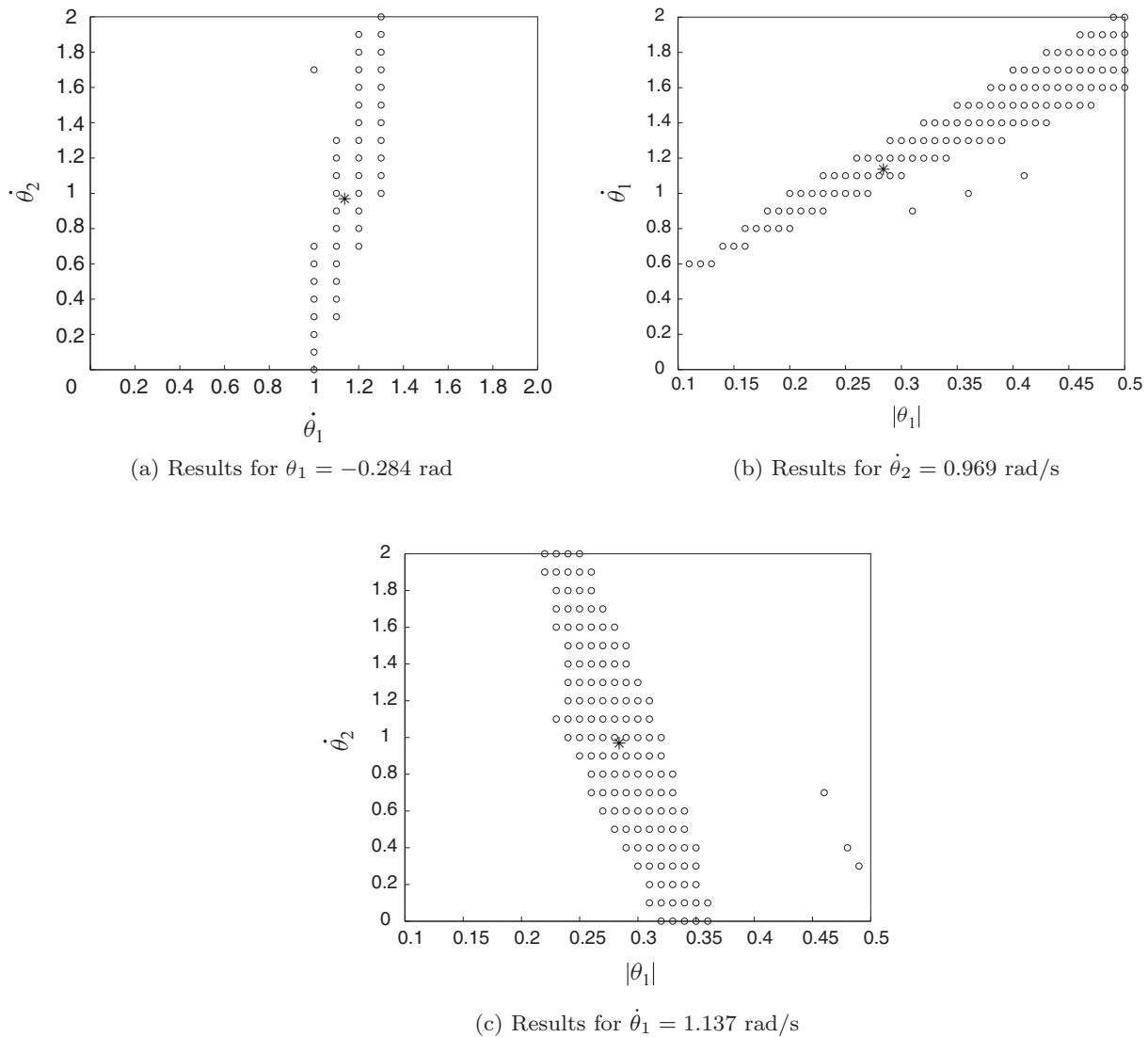


Fig. 18. Basin of attraction.

reference trajectory were clarified and the proposed method could decrease shin mass and foot radius of the biped robot. In particular, SR became one-fifth of the most minimum value of forward bending walking,⁷ and the semicircular feet could be removed. In the future work, we will clarify the reason why inverse bending walking is analytically more than efficient than forward bending walking.

References

1. T. McGeer, "Passive dynamic walking," *Int. J. Robot. Res.* **9**(2), 62–82 (1990).
2. A. Goswami, B. Espiau and A. Keramane, "Limit cycles in a passive compass gait biped and passivity-mimicking control laws," *J. Auton. Robots* **4**(3), 273–286 (1997).
3. F. Asano, M. Yamakita and K. Furuta, "Virtual Passive Dynamic Walking and Energy-Based Control Laws," *IEEE/RSJ International Conference on Intelligent Robotics and Systems*, (Oct. 31–Nov. 5, 2000) pp. 1149–1154.
4. F. Asano, Z.-W. Luo and S. Hyon, "Parametric Excitation Mechanisms for Dynamic Bipedal Walking," *IEEE*

- International Conference on Robotics and Automation* (Apr. 18–22, 2005) pp. 611–617.
5. F. Asano and Z.-W. Luo, "Energy-efficient and high-speed dynamic biped locomotion based on principle of parametric excitation," *IEEE Trans. Robot.* **24**(6), 1289–1301 (2008).
6. F. Asano, T. Hayashi, Z.-W. Luo, S. Hirano and A. Kato, "Parametric Excitation Approaches to Efficient Bipedal Walking," *Proceedings of the 2007 IEEE/RSJ International Conference on Intelligent Robots and Systems* (Oct. 29–Nov. 2, 2007) pp. 2210–2216.
7. Y. Harata, F. Asano, Z.-W. Luo, K. Taji and Y. Uno, "Biped gait generation based on parametric excitation by knee-joint actuation," *Robotica* **27**(07), 1063–1073 (2009).
8. M. W. Spong, "The swing up control for the acrobat," *IEEE Control Syst. Mag.* **15**(2), 49–55 (1995).
9. E. K. Lavrovskii and A. M. Formalskii, "Optimal control of the pumping and damping of swing," *J. Appl. Math. Mech.* **57**(2), 311–320 (1993).
10. F. Asano and Z.-W. Luo, "The Effect of Semicircular Feet on Energy Dissipation by Heel-Strike in Dynamic Bipedal Locomotion," *IEEE International Conference on Robotics and Automation* (Apr. 10–14, 2007) pp. 3976–3981.